Results in Engineering 27 (2025) 106931

Contents lists available at ScienceDirect

Results in Engineering

journal homepage: www.sciencedirect.com/journal/results-in-engineering

Research paper

Machine learning-assisted design automation workflow of non-uniform flow distributors for multipass crossflow device

Mertcan Kaya [a,*], Julian Ferchow [b], Mirko Meboldt [c], Christoph Klahn [a,d]

[a] Karlsruhe Institute of Technology (KIT), Institute for Micro Process Engineering (IMVT), 76344 Eggenstein-Leopoldshafen, Germany
[b] Inspire AG (ipd|z), 8092, Zürich, Switzerland
[c] ETH Zurich (pd|z), 8092, Zürich, Switzerland
[d] Karlsruhe Institute of Technology (KIT), Institute of Mechanical Process Engineering and Mechanics (MVM), 76131 Karlsruhe, Germany

ARTICLE INFO

Keywords:
ML driven design
Design automation
Chemical engineering
Additive manufacturing
Flow distribution
Bifurcation design

ABSTRACT

Multipass crossflow devices are essential in the process engineering industry due to their broad range of applications. The growing use of additive manufacturing techniques offers opportunities to improve the efficiency of these devices by enabling non-uniform flow distribution, which can enhance heat transfer uniformity to avoid temperature gradients across individual channels in chemical engineering applications such as heat exchangers and packed bed reactors. This paper addresses the challenge of controlling non-uniform flow distribution by developing a novel design that locally varies channel diameters at predefined positions within the distributor, to achieve user-defined target flow distribution ratios. The proposed design combines machine learning-assisted design automation workflow with algorithmic modeling and computational fluid dynamics (CFD) simulations to manage the complexity of non-uniform flow distribution effectively. The results are further validated through an experimental study of an incompressible gas flow distributor, which supports the findings presented in this work.

1. Introduction

Multipass crossflow devices, such as heat exchangers, are widely employed in process engineering for heating and cooling applications. The selection of a suitable flow arrangement depends on multiple factors, including thermal efficiency, fluid paths, space constraints, temperature levels, and production costs [1–3]. Owing to their compact design, multipass crossflow heat exchangers offer significant advantages in industrial settings. However, their optimal performance depends on maintaining a uniform heat transfer coefficient across all channels, which is strongly influenced by the inlet flow distribution [4–7]. Even slight deviations in channel flow can create local variations in heat transfer coefficients, particularly in microchannel exchangers, thereby degrading thermal performance compromising the overall thermal performance of the system [5]. Notably, Guo et al. demonstrated that, under specific conditions, controlled non-uniform flow can enhance heat transfer [4]. This strategy enhances overall heat transfer while promoting uniform heat transfer across all channels through a controlled, non-uniform flow distribution [8]. Such enhancements are beneficial not only for multipass crossflow heat exchangers but also for crossflow reactors used in exothermic processes. Isothermal conditions in these reactors enable higher conversion rates, emphasizing the importance of isothermal crossflow devices in these applications [9]. These findings highlight the broad applicability of controlled non-uniform flow distribution in devices ranging from heat exchangers to chemical reactors and separators. Achieving optimal flow distribution in such devices depends on the implementation of carefully designed and application-specific flow distributors.

Consecutive configurations, such as U-type and Z-type, have been extensively studied due to their simplicity and compactness in addressing flow distribution challenges [10,11]. Both designs exhibit similar inlet flow characteristics, differing mainly in outlet direction: the U-type reverses flow, while the Z-type maintains its direction (see Fig. 1). Research on these distributors primarily targets flow uniformity [12–14], supported by analytical methods for design and optimization [12,15]. Their performance depends heavily on geometric factors, including branch number, channel diameter, and baffle design [12,16]. However, as channel count increases, these distributors become increasingly vulnerable to uncontrolled maldistribution [17,18].

Bifurcation geometries offer a promising alternative, particularly with advances in additive manufacturing (see Fig. 1). These structures have demonstrated a strong ability to minimize maldistribution across

* Corresponding author.
E-mail address: mertcan.kaya@kit.edu (M. Kaya).

https://doi.org/10.1016/j.rineng.2025.106931
Received 29 June 2025; Received in revised form 7 August 2025; Accepted 25 August 2025

Available online 3 September 2025

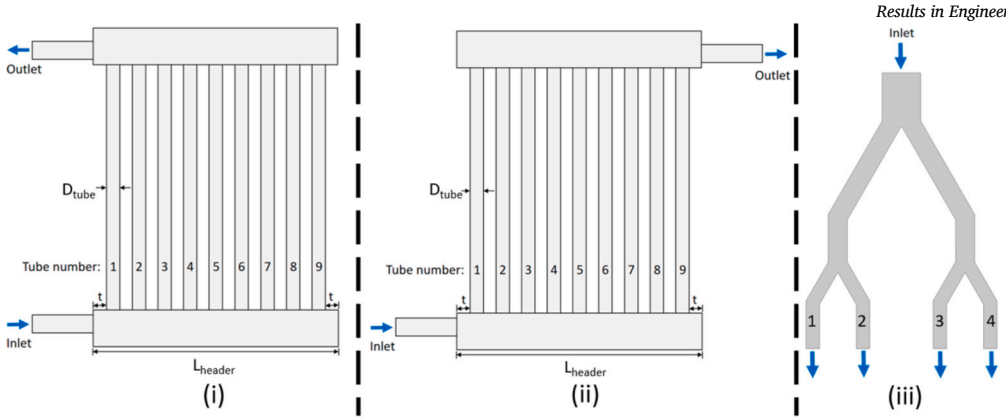

Fig. 1. Typical flow distribution designs: (i) U-type, (ii) Z-type arrangements of parallel channel flow distributors [19] and (iii) bifurcation flow distributors.

various applications [20–22]. Unlike consecutive manifolds, bifurcation designs maintain uniform flow across a wide range of flow rates, including high Reynolds numbers, making them robust under fluctuating operating conditions [11]. Their performance is largely governed by parameters such as bifurcation angle, number of stages, and outlet edge length [20,23–25]. Analytical frameworks, such as the one proposed by Mazur et al. [20], have improved flow uniformity by optimizing these parameters. However, current studies primarily focus on uniformity and rarely explore the deliberate control of non-uniform flow and its potential benefits.

Developing distributors that intentionally manipulate non-uniform flow requires precise mass flow control to ensure uniform residence times and maximize thermal performance. Bury & Hanuszkiewicz-Drapała showed that directing controlled flow to regions with higher temperature gradients can improve efficiency by up to 23.3% compared to uncontrolled non-uniform flow and by up to 6.5% over uniform flow conditions [26]. Similarly, Gao et al. demonstrated the ability to manage non-uniform distributions by leveraging induced vortices [8]. Despite these benefits, controlling non-uniform flow distribution introduces additional geometric parameters, enlarging the solution space and increasing computational demands to identify the global optimum. To the best of our knowledge, research on advanced optimization algorithms for this purpose remains limited, whereas machine learning (ML)–assisted approaches have demonstrated considerable potential in design optimization. For instance, Lira et al. proposed an artificial neural network (ANN) optimized using a genetic algorithm to enhance micro-photocatalytic reactor designs with computational fluid dynamics (CFD) [27]. Similarly, Koide et al. trained convolutional neural networks (CNN) using a random walk algorithm to explore the solution space and predict heat transfer in fluid flow [28]. Both studies successfully demonstrated the ability of these deep learning algorithms to predict design behavior. However, methods like ANN and CNN require large datasets for training, resulting in significant computational time [29,30]. In another application, Owoyele et al. demonstrated a developed ML method using genetic algorithm in engine design optimization problem [31]. Their method employed 200 initial CFD simulations to train a surrogate model with exclusive hyperparameter optimization. While this approach highlights the advantages of ML in design optimization, the high number of initial simulations remains a challenge. Gradient-based methods offer a viable alternative, especially when the number of design parameters is greater than the number of objectives [32,33]. However, they come with the risk of getting trapped in local minima [34].

To address this limitation, Morita et al. proposed a Bayesian Optimization (BO) method based on Gaussian Process Regression (GPR) to optimize the shape of the upper wall of a two-dimensional channel [34]. This approach significantly reduced the number of required CFD simulations, solving an optimization problem with up to eight parameters using only 90 simulations. BO, a heuristic-based search algorithm, effectively finds the optimum value with minimal data input [35], making it well-suited for optimizing computationally expensive black-box functions [36]. By constructing a probabilistic surrogate model using GPR, BO efficiently balances exploration of uncertain regions and exploitation of promising areas [37]. To initialize the surrogate model, a Latin Hypercube Sampling (LHS) strategy is often employed, ensuring that the initial samples are well-distributed across the solution space [38].

Building on these insights, we propose a comprehensive design automation workflow that integrates ML techniques to achieve precise control of non-uniform fluid flow distribution while minimizing design and optimization effort. The workflow enables automated development and optimization of flow distribution structures, introduces innovative solutions to enhance thermal performance, and establishes a foundation for future implementation of more complex distributor designs through developed automation workflow. The key contributions of this paper are as follows:

- A novel ML-driven automation workflow for designing and optimizing flow distribution structures, ensuring improved performance, efficiency, and reduced human effort.
- Experimental validation of the proposed workflow, demonstrating its practical applicability and effectiveness in achieving the desired flow control.

This paper is organized as follows: The section 2 proposes a new automated design workflow for non-uniform flow distribution. The provided workflow is supported by an experimental work to validate used CFD simulation, defined in Section 3. The Section 4 presents and discusses the results of the experimental work, highlighting the workflow's applicability.

2. Proposed ML-assisted design automation workflow of flow distributor

The primary goal of this paper is to develop a workflow to design and optimize flow distribution according to user-defined distribution ratios in each channel, thereby making the advantages of non-uniformity in flow distribution available. To achieve this objective and demonstrate the workflow's effectiveness, we focused on incompressible gas flow distribution systems operating under turbulent flow conditions. The objective function of the optimization process is defined to minimize the deviation between the actual distribution and the user-defined ratios. In this workflow, the optimization is performed by morphing the channel diameters at predefined positions within the distributor, the details of which are presented in Section 2.1.

2.1. Algorithmic design of flow distributor

As a starting point, the distribution structures discussed in Section 1 are analyzed and compared. Bifurcation distributors offer greater scala-

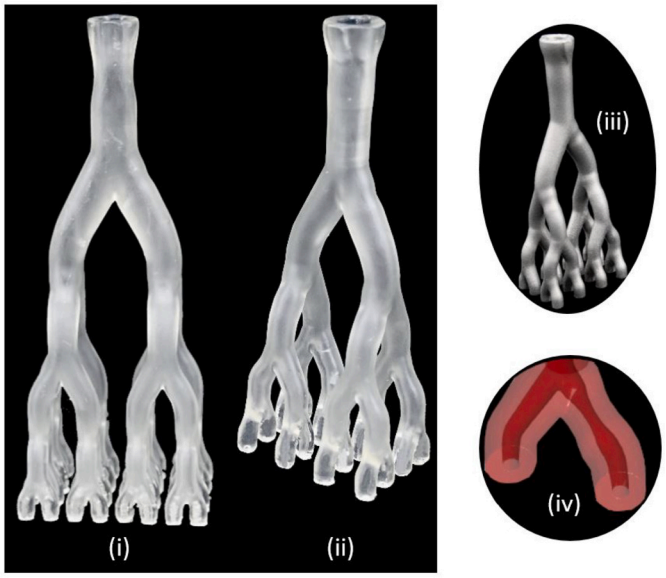

Fig. 2. Additive manufactured morphed bifurcation type flow distributors: Design variants with (i) 64 channels, (ii) 16 channels, (iii) 16-channel metal design manufactured with PBF-LB/M method, and (iv) detailed view of the morphed structure.

bility in three dimensions compared to consecutive distributors, which provides more potential for applications in multipass crossflow devices. This characteristic makes bifurcation structures more suitable for controlling gas flow distribution across multiple channels in complex systems. Creating complex flow distributor designs, such as bifurcation geometries, is only feasible through additive manufacturing. Techniques like laser-based powder bed fusion of metals (PBF-LB/M) and vat-based photopolymerization of polymers using ultraviolet light (VPP-UVL/P) allow for intricate designs and provide the ability to precisely control fluid flow within channels. Leveraging these capabilities, we developed a workflow to control flow distribution using morphing channels within bifurcation flow distributors. The manufacturability and scalability of various morphed flow distributor configurations were validated using both additive manufacturing methods (see Fig. 2).

To analyze turbulent fluid flow behavior within bifurcation type flow distributors, the volumetric flow rate (Q) can be calculated using Swamee and Jain equation, specifically designed to define the volumetric flow rate [39]:

$$Q = -0.965 \left(\frac{g D^5 h_L}{L} \right)^{0.5} \ln \left[\frac{\varepsilon}{3.7D} + \left(\frac{3.17 \nu^2 L}{g D^3 h_L} \right)^{0.5} \right] \quad (1)$$

This equation highlights the dependence of the volumetric flow rate (Q) on key parameters such as the channel diameter (D), the head loss (h_L), the channel length (L), the channel roughness (ε), and the fluid kinetic viscosity (ν). By managing head loss through pressure differences and morphing the diameter of each channel, the mass flow distribution between channels can be controlled. Controlling flow distribution in a bifurcation system with n branches requires $n-1$ morphing positions (see Fig. 3). Consequently, the number of required morphing positions increases significantly as the number of stages in classical 2^n bifurcation distributors grows. This complexity makes traditional methods of design exploration, such as simplified analytical approaches or intuition-based adjustments, impractical for accurately optimizing morphing diameters. To overcome these limitations, CFD simulations are employed to systematically analyze flow distribution and explore design variants. The complex interplay between morphing diameters and optimization objectives makes it essential to employ an automated workflow for efficiently designing and evaluating multiple bifurcation structure variants.

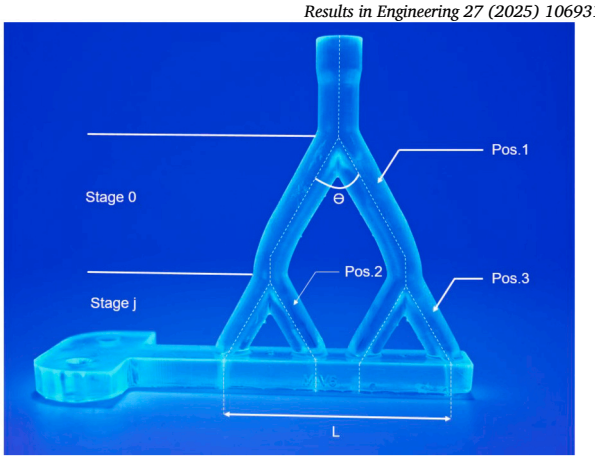

Fig. 3. Morphed flow distributor design for validation tests using design parameters: bifurcation angle (Θ), stage number (j), outlet stage edge length (L) and morphing positions (Pos.), photographed under UV light.

Combining design automation with simulations makes optimization with high number of parameters feasible [40,41]. To develop a design automation workflow for flow distributors, it is essential to define the bifurcation geometry through unambiguous design parameters. These parameters must accurately describe the geometry and remain stable during changes to prevent errors when the automation begins. Therefore, the parameters and formulas provided by Mazur et al. [20] are integrated into the design to ensure a robust model within *Rhinoceros/Grasshopper* software.

Additionally, an algorithmic model has been developed to enhance flexibility, allowing the same design framework to accommodate various channel numbers. In the creation of the bifurcation design model, several parameters are used to define the bifurcation, including the bifurcation angle (Θ), the outlet diameter of the last stage, the stage number (j), the outlet stage edge length (L) and the wall thickness [20]. These parameters, while critical to the design, are fixed during the automated parameter optimization. This approach is specifically adopted to accelerate and simplify the optimization process, enabling efficient and fast design optimization using validated literature design. The optimization relies solely on the morphing diameters at each morphing position, as illustrated in Fig. 3. To define these diameters in the algorithmic model, morphing parameters with predefined ranges are introduced, where the lower limit of 0 indicates no morphing, and the upper limit corresponds to the minimum acceptable morphing diameter. This upper limit is determined experimentally to ensure consistency between CFD simulations and experimental measurements. As indicated by Equation (1) and supported by An et al. [42], a significant reduction in channel diameter increases hydraulic resistance and causes unpredictable flow distribution, highlighting the necessity of defining this limit to maintain stable operation within the workflow.

2.2. CFD model

Flow simulation is conducted using the CFD software *StarCCM+* to evaluate variations in the bifurcation design. To accurately define the design, hexagonal meshes with prism layers at the boundaries are used, and an automated mesh generation process is implemented within the software. A mesh sensitivity analysis is conducted by gradually coarsening the mesh until results deviate significantly, ensuring a balance between accuracy and computational efficiency.

The shear stress transport (SST) k-ω turbulence model is selected for this study due to its superior performance in capturing near-wall effects, making it suitable for the flow distributor design being analyzed [20]. While the k-ω model offers significant advantages for near-wall applications [43], the standard k-ϵ model predicts flow behavior accurately in curved channels [44]. Given the small diameters of the flow

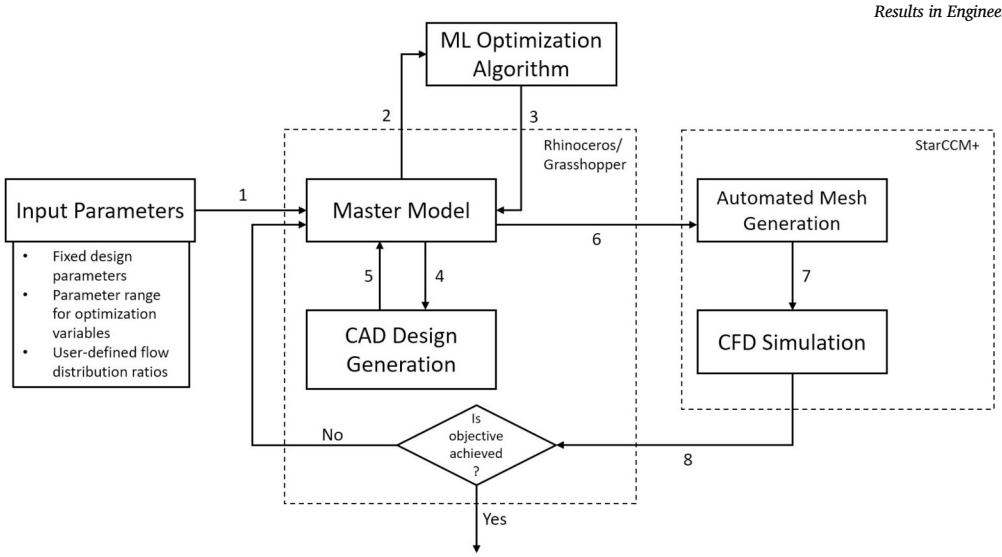

Fig. 4. Sequential numbering of the design automation workflow steps.

distributor channels used in this research, near-wall effects play a crucial role. Therefore, the SST k-ω model is selected for its accuracy in near-wall regions, while still incorporating the benefits of the k-ϵ model for predicting flow in curved channels. This ensures accurate simulation of boundary layer behavior and enhances the definition of the overall flow dynamics in the design. Additionally, the different surface roughness caused by PBF-LB/M method compare to VPP-UVL/P and machining parts [45,46], is treated properly with SST k-ω model.

Within the specified convergence criteria referenced from [20], the simulation solves the steady state Reynolds averaged Navier–Stokes equations until the mass flow changes in each channel smaller than 10^{-6} g/s. Finally, the CFD model is validated with the additive manufactured test parts using pressurized air in hot wire anemometer.

2.3. Automated design optimization assisted by machine learning

As discussed in Section 2.1, the design variables for the optimization problem are determined by the number of morphing positions. The objective function is defined to minimize the deviation between the actual flow distribution and the user-defined target ratios. To proceed, the input parameters include fixed design parameters, as shown in Fig. 3, the parameter range for the optimization variables, and the target flow distribution ratios provided by the user. The optimization problem is then solved using CFD simulations to analyze gas flow distribution under turbulent flow conditions, as described in Section 2.2. The subsequent step involves setting up an automated data exchange system between the design and simulation software, ensuring seamless integration and enhancing the efficiency of the optimization process.

Effective data exchange between design and simulation software is essential for a successful design automation workflow. To achieve this, a master model (MM) is required [40,47]. The MM facilitates structured, sequential communication between the design and simulation software. As illustrated in Fig. 4, the user defines the ranges for optimization variables, target distribution ratios and provides fixed design parameters (1). With code using *C#* programming language embedded in *Rhinoceros/Grasshopper* software, MM communicates with the ML optimization algorithm in *Python* (2,3) to adjust the optimization variables and initiates the design software to generate the necessary files for simulation (4,5). Upon exporting these files, the MM activates the simulation software to retrieve mass flow results for each channel (6). *StarCCM+* software meshes the generated design automatically and starts the CFD simulation (7). Subsequently, the MM compares the mass flow distribution across channels with the target values, identifying deviations (8). The process of adjusting optimization variables is repeated in subsequent iterations until the defined maximum iteration limit is reached or the target value is smaller than a user-defined threshold.

This proposed design automation workflow is developed specifically to minimize deviations from the target mass flow distribution in channels, offering flexibility to accommodate different optimization algorithms. It is possible for users to choose from advanced optimization techniques to find the global minimum. To enhance flexibility and efficiency in the flow distributor optimization, we implemented Bayesian Optimization (BO) with a Gaussian Process Regressor (GPR) using *Python*'s *Scikit-learn* library within the design automation workflow. In our context, the optimization problem is viewed as an expensive black-box function due to long iteration time and unknown relationships between input and output parameters in especially complex distributor designs. Given these challenges, BO proves to be a valuable approach, as it efficiently explores the solution space while minimizing computational costs, as discussed in Section 1.

The optimization problem for the n-channel flow distributor involves n-1 input morphing parameters and n mass flow distribution outputs at the outlet channels. This characterizes the problem as multi-objective. Due to the single-objective optimization nature of BO, it requires a scalarization function to address the multi-objective nature of this problem [48].

To achieve this, the Chebyshev scalarization method is applied, which is defined as [49]:

$$f_{Chebyshev}(x) = \max_{i=1,\ldots,n} \left(\lambda_i \left| f_i(x) - z_i^* \right| \right). \tag{2}$$

The parameter set for each iteration is denoted as x, where $f_i(x)$ represents the relative deviations. Since the mass flow distribution in all channels is equally important, the weights λ_i are set to $\frac{1}{n}$ for each objective to avoid favoring any one output. Additionally, the ideal values (z_i^*) are set to 0, aligning with the goal of minimizing the relative deviations between the actual flow distribution and the user-defined target ratios as much as possible. By using the Chebyshev scalarization function, the multi-objective problem is transformed into a single-objective optimization problem. The overall goal is to minimize $f_{Chebyshev}$, ideally bringing it below 0.25%, which we consider an acceptable level for this optimization task.

Additionally, multipass crossflow devices are widely used and essential across various applications, each with unique design requirements. The design automation workflow applies to optimizing the same design for different requirements, making the collected data highly valuable for future optimal configurations in flow distributor design. For this reason, the results from each optimization case are stored in a CSV file for sub-

sequent use. It should be noted, however, that data from a previous optimization case are only transferable when the bifurcation number of the flow distributor is identical in both cases. To enhance BO further, we incorporated LHS and GPR (see Section 1). LHS, a widely used method for solution space exploration, efficiently covers the solution space with fewer iterations than classical random sampling methods. After the initial sampling, a GPR is trained to predict likely areas of global minimum, which it then connects to the BO. Following this first sampling phase, we adjusted the optimization workflow to favor exploitation over exploration using the Lower Confidence Bound (LCB) acquisition function, helping to refine the search within identified regions. These adjustments in the optimization algorithm reduce computational time, particularly when initial values are available from previous optimization cycles.

3. Experimental validation

3.1. Design and manufacturing of test device

The algorithmic design of the flow distributor can be adjusted for different numbers of channels by modifying the fixed parameter of bifurcation stages (j) in the design automation workflow (see Fig. 2). To validate the flow distributor design workflow proposed in Section 2 and its optimization algorithm to control flow distribution ratios, a four-channel flow distributor is used as a two-dimensional design, as shown in Fig. 3. In the test design, the bifurcation angle (Θ) is set to 30°, the outlet stage edge length (L) is fixed at 20 mm, the number of stages is set to 2, the wall thickness is maintained at 2 mm, and the outlet diameter of the final stage is specified as 2 mm. This approach allows for a comprehensive and efficient validation of the methodology. In addition to the bifurcation geometry, a bottom section is incorporated into the design to secure the part during testing, as shown in Fig. 3. The part is fixed in place, and to ensure flatness, an L-shaped feature is added to the geometry. This feature allows the use of a spirit level to verify that the part remains level throughout the process.

To assess the impact of manufacturing tolerances, the validation designs were produced using the PBF-LB/M and VPP-UVL/P additive manufacturing methods. Both methods offer effective solutions for manufacturing complex structures. In the VPP-UVL/P process, a photosensitive resin is placed in a vat, and UV light selectively solidifies the resin layer by layer through polymerization [46]. Since printed parts are fragile, post-processing is essential in this method and varies depending on the resin material used. Typically, removable support structures are printed alongside the part to ensure production stability. These support structures can be easily removed manually after printing. The next post-processing step involves washing the structure with isopropanol to remove any uncured resin [50]. After this, the part is cured under UV lights until fully solidified. It's crucial to remove all uncured resin and isopropanol from the printed part to achieve precise manufacturing tolerances. The PBF-LB/M process enables metal additive manufacturing by using laser power to selectively melt metal powder layer by layer [46]. However, post-processing is more tedious because the support structures cannot be easily removed by hand; they must be cut or removed through machining operations. If the support structures are inside the part's internal geometry, removal becomes impossible. Therefore, it is essential to minimize the use of support structures and fully understand the design limitations of this manufacturing method. Several studies in the literature have explored the design limitations of the PBF-LB/M method [46,51–53]. These limitations depend on the material used, process parameters, and the machine. In this study, stainless steel 316L was used as the printing material, and the design guidelines reported by multiple resources are followed in the design of flow distributor [46,51,52].

To experimentally define the diameter boundaries that ensure reliable correlation between CFD simulations within the proposed workflow and experimental results, as discussed in Section 2.1, seven variations of the validation flow distributor (see Fig. 3) were created and manufactured using both VPP-UVL/P and PBF-LB/M methods (see Table 1). Variant identifiers follow the format N-V_x or M-V_x, where 'N' stands for an unmodified channel, 'M' for a modified channel including local diameter reductions and 'V_x' for the specific variant number. Two parts without morphing parameters (N-V1) were produced to compare the CFD simulation with experimental data in cases of uniform flow distribution. Subsequently, the workflow's boundaries were further explored by morphing the structure in extreme cases with smaller diameters. The diameters of the morphed positions are increased in each variant after testing extreme cases (e.g. M-V1). Additionally, the effect of the morphing positions is also investigated in the validation process.

Table 1
Minimum channel diameters at the different morphing positions, as defined in Fig. 3, are listed for each test part.

Variation	Minimum Morphing Diameter (mm)		
	Pos. 1	Pos. 2	Pos. 3
N-V1	-	-	-
M-V1	0.682	0.670	0.670
M-V2	0.907	0.830	0.830
M-V3	0.907	-	-
M-V4	1.227	-	-
M-V5	0.840	-	-
M-V6	0.840	0.765	0.765

3.2. Test set-up

Experiments were conducted to validate the CFD model using a hot wire anemometer (HWA), a valuable tool for determining flow distribution [54]. HWA measures flow velocity by detecting temperature changes: as gas flows over a heated wire, the wire cools, and the anemometer adjusts the current to maintain a constant temperature. The rate of current change correlates with the fluid's velocity. However, HWA is highly sensitive to movement, so stabilizing the test part using a motion control system is essential for accurate measurements.

In the test setup, pressurized air is used as the flow medium, and the mass flow rate is regulated at 0,169 g/s throughout the validation process using a mass flow controller from *Brooks Instrument*. The air is directed into the test part, with a straight, rigid pipe (i) positioned in the forward direction (see Fig. 5). This configuration is critical, as even minor deviations can significantly impact the flow distribution. To secure the part, two aluminum profiles are attached to the movement system (ii) from *Physik Instrumente*. The test part is first assembled into the setup using screws and the aluminum profiles (iii). The inlet pipe and test part are connected and sealed with a rubber gasket (iv). After pressurizing the system, leak detection spray is used to check for leaks. Once the system is confirmed to be leak-tight, the test part is brought near the HWA (v) by moving it along the left-right axis to improve measurement accuracy. After this, the part is moved along the up-down and forward-backward axis by 0.2 mm/s to identify the highest flow rate detected by the HWA and collect accurate data. Mass flow rates are calculated using the measured outlet diameters of the channels and the air density in normal conditions.

To ensure repeatability, each test part is measured twice using HWA. Additionally, they are disassembled, reassembled, and tested a third time to account for any effects from assembly. The pressure difference across the test part is measured using pressure differential equipment (vi) from *WIKA*.

4. Experimental results

To establish the functionality boundaries of the workflow and validate the CFD model, 14 test parts were printed and tested as detailed in

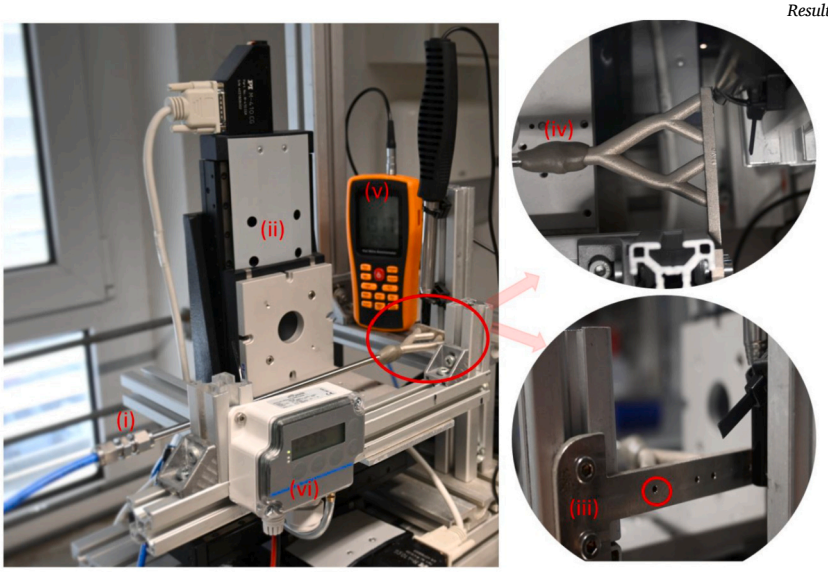

Fig. 5. Test set-up for performance tests and to validate CFD model highlighting rigid pipe (i), motion system (ii), assembly mechanism and measurement outlets (iii), sealing rubber gasket (iv), hot wire anemometer(v), pressure differential equipment (vi).

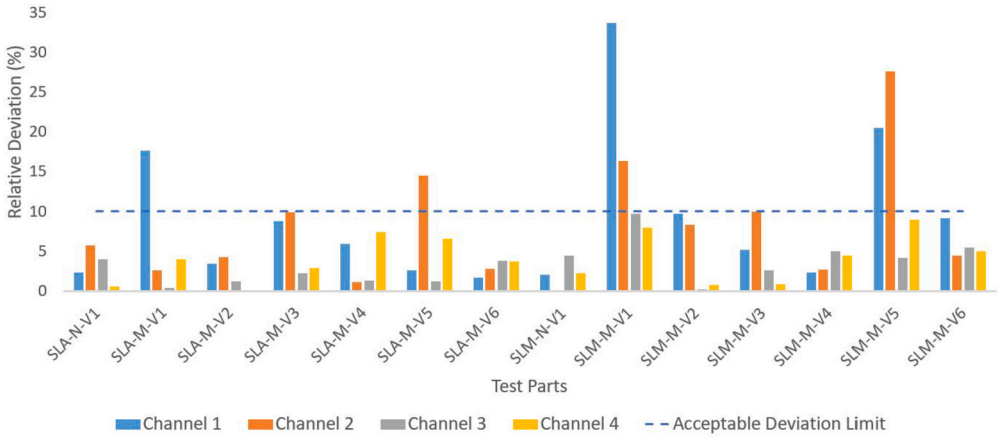

Fig. 6. Error in comparison between experiment and simulation data based on corresponding 3D-CAD Model.

Table 1 and Fig. 3. Due to the novelty of incorporating non-uniformity in flow distributors, classical quality assurance parameters such as the general deviation from uniformity parameter (β) and the worst-case maldistribution parameter (ξ), as described in the literature [23,55], are not applicable. However, the relative deviation, which is derived from the core concept of ξ, can be defined as:

$$Relative\ Deviation = \frac{\sum_{i=1}^{n}\left(U_{sim,i} - U_{exp,i}\right)}{\sum_{i=1}^{n} U_{exp,i}} \times 100\% \quad (3)$$

Where $U_{sim,i}$ represents the mass flow distribution ratio at location i from the simulation, $U_{exp,i}$ denotes the mass flow distribution ratio at location i from the experiment, and n is the total number of measurements.

Using this formula, the relative deviations were calculated for each channel in the test parts. Based on maldistribution parameter (ξ) values reported in the literature [23,55,56], which demonstrate designs achieving a relative deviation below 10%, this study adopts 10% as the acceptance criterion for flow distribution. Due to the low pressure drop values observed, they can be considered negligible at least for the size of test parts. Even in the extreme reduced diameter case of M-V1 (see Table 1), the maximum pressure drop reached only 390 Pa.

4.1. Boundaries of using the morphing method

As discussed in Section 2.1, a sharp reduction in channel diameter leads to unpredictable flow behavior, resulting in deviations between experimental measurements and simulation results. Based on the comparison of experimental data with simulation results, the acceptable minimum channel diameter for this workflow is identified, ensuring that the workflow remains valid only within this experimentally confirmed range. Fig. 6 presents the relative deviation values for all tested parts, where SLA refers to parts manufactured by VPP-UVL/P and SLM refers to those produced by PBF-LB/M. The raw experimental and simulation datasets used to calculate the relative deviation values using Equation (3) shown in Fig. 6 are provided in the Supplementary Information.

The relative deviation for the smallest diameter cases, M-V1 and M-V5 (see Table 1), exceeds the acceptance limit of 10%. For M-V1, the variant manufactured by VPP-UVL/P reached a maximum deviation of 17%, whereas the metal version produced by PBF-LB/M exhibited a deviation of 33%. In the case of M-V5, deviations also exceed the limit, despite the first morphing position having the same diameter as in M-V6 (see Table 1). This finding indicates that applying morphing at each bifurcation stage, as in M-V6, regulates the flow distribution more effectively and allows the use of smaller diameters compared to modifying only the first position, as in M-V5. Nevertheless, for applications

Table 2
Summary of iteration results for variants with target ratios and computational requirements.

Case Number	Variant Name	Target Ratios	Exploration Iterations	Exploitation Iterations	$f_{Chebyshev}$	Required Time (h)
1	M-V2	0.18, 0.22, 0.26, 0.34	60	11	0.0091	~4
2	M-V4	0.24, 0.23, 0.24, 0.27	30	27	0.1440	~3.5
3	N-V1	0.25, 0.25, 0.25, 0.25	30	19	0.2100	~3
⋮	⋮	⋮	⋮	⋮	⋮	⋮
9	M-V11	0.20, 0.24, 0.26, 0.30	-	-	0.2320	In seconds

Fig. 7. Comparison between VPP-UVL/P and PBF-LB/M manufactured parts.

requiring lower sensitivity to non-uniformity, reducing the number of morphing positions can be advantageous, as it decreases the number of optimization variables and thereby lowers computational cost while improving the efficiency of the design automation workflow. As illustrated in Fig. 6, the relative deviation between simulations and experiments for all variants except M-V1 and M-V5 remains within the acceptable threshold. Among the tested designs, M-V6 with a diameter of 0.84 mm in the first morphing position and 0.765 mm in the second and third positions, represents the smallest channel dimensions that maintained acceptable flow distribution deviations across both manufacturing methods.

According to the experimental data, there is a slight difference between the parts manufactured using VPP-UVL/P and PBF-LB/M (see Fig. 7), both of which are within the acceptable relative deviation range. However, it is important to note that process parameters have a significant impact on manufacturing quality, particularly for parts produced using PBF-LB/M. Parameters such as part orientation, laser power, scanning speed, hatch spacing and layer thickness play a crucial role in determining manufacturing tolerances and surface quality [57]. Therefore, it is crucial to characterize the manufacturing machine if operating close to the workflow boundaries. Variations in machine settings and parameters can shift these boundaries. Additionally, the reduction in size after post-processing, such as milling, must be taken into account for PBF-LB/M parts.

4.2. Effect of used ML-assisted optimization algorithm

As described in Section 2.3, the proposed design automation workflow optimizes the flow distributor to achieve the desired mass flow distribution. Supervised ML method Gaussian Process Regressor is used to enhance the prediction for Bayesian Optimization to minimize the deviation in mass flow distributions in the flow distributor design. To demonstrate the effectiveness of the proposed workflow, the target ratios and simulation results for different cases were used (see Table 2). The optimization algorithm begins with an exploration phase, where the solution space is broadly sampled, and then transitions to an exploitation phase, focusing on areas likely to yield optimal results. To ensure comprehensive exploration, 60 sampling iterations are performed using LHS, generating sufficient data to map the solution space for the input parameters. This sampled data is then used to train the GPR model, which collaborates with BO to refine the search, prioritizing regions with a higher probability of containing the optimal solution. After the initial exploration, BO performs up to 30 additional iterations to optimize the design. Each iteration, including design and simulation of test flow distributors, requires approximately 3.5 minutes on a 12-CPU setup. Since the bifurcation number of the test flow distributors remain constant across all cases defined in Table 2, the data from each optimization case are stored in a CSV file and imported prior to the sampling phase in subsequent cases to train the GPR model. This transfer of prior knowledge facilitated faster exploration of the solution space and reduced the number of required simulations in later cases. Further implementation details, including hyperparameter configurations for BO and GPR, are provided in the Supplementary Information. In the following, the application of the optimization algorithm to the different cases defined in Table 2 is presented to illustrate its performance under varying target distributions.

The M-V2 optimization problem was solved in 71 iterations over approximately 4 hours. The algorithm successfully minimized $f_{Chebyshev}$ (as detailed in Section 2.3) to 0.0091, completing the optimization cycle. The evaluated data points and their simulation results were then saved to a CSV file for use in subsequent optimization case.

In another optimization case with different target mass flow distribution ratios, the M-V4 variant was applied using three input parameters. By leveraging initial samples from the earlier M-V2 variant, the optimization process for M-V4 was configured with 30 sampling iterations and 30 exploitation iterations. Upon completing the sampling phase and 27 exploitation iterations, the algorithm successfully reduced the $f_{Chebyshev}$ value to 0.144. The optimization cycle stopped based on a stopping criterion of <0.25, defined in Section 2.3. This problem was solved in approximately 3,5 hours. By focusing on the observed region of the solution space, the required number of simulation iterations can be significantly reduced. We estimate that 500 iterations are sufficient to define the solution space for three input parameters, similar to the case of the four-channel flow distributor. This estimate is supported by the use of LHS, which ensures a well-distributed exploration of the solution space during each optimization case. LHS provides comprehensive coverage, which is particularly effective given the relatively low dimensionality of the solution space with three input parameters.

Once 500 iterations are completed, the surrogate model (GPR) takes over, and further simulations are no longer triggered by the MM. Instead, the optimization process relies entirely on GPR predictions, reducing computation time to just a matter of seconds. The M-V11 variant serves as a case study to demonstrate the functionality of the surrogate model within the optimization framework. Using the GPR model, the surrogate successfully identified an $f_{Chebyshev}$ value of 0.232 in seconds (see Table 2). This strategy significantly improves efficiency for a widely used design across various applications, while preserving the accuracy of the optimization results.

5. Discussion

The results of the ML-assisted design optimization and experimental validation demonstrate that the proposed workflow effectively controls flow distribution to match user-defined ratios. This capability addresses the challenge of non-uniformity in multipass crossflow devices

and provides a solid foundation for future enhancements in heat transfer uniformity in individual channels. While this study focuses on flow distribution control, the workflow has the potential to be extended to heat transfer applications and the implementation of more complex flow distribution designs in future work.

The current implementation is most effective for systems with a moderate number of channels. However, as the number of channels increases, computational times for optimization also grow. To mitigate this, the integration of specialized ML models into the design automation framework in the future could substantially enhance computational efficiency. The flexibility of the proposed system also supports the integration of alternative ML algorithms, as discussed in Section 2.3, making it adaptable to more complex flow distributors and sophisticated systems.

6. Conclusion

This paper introduces a design automation workflow utilizing machine learning assisted algorithms to optimize non-uniform flow distribution in multipass crossflow devices. The findings demonstrate that strategically morphing channel geometries can effectively control flow distribution. However, the applicability of this workflow is constrained by the tolerances inherent to the selected manufacturing techniques. The proposed automation workflow enables flexibility through advanced optimization algorithms and different machine learning methods, with substantial reductions in optimization time achievable, particularly when initial values from prior optimization cycles are available. This design automation workflow and the non-uniform flow distribution strategy show promising potential for application across various process engineering devices.

CRediT authorship contribution statement

Mertcan Kaya: Writing – original draft, Validation, Methodology, Investigation, Conceptualization. **Julian Ferchow:** Writing – review & editing, Supervision. **Mirko Meboldt:** Supervision. **Christoph Klahn:** Writing – review & editing, Supervision, Funding acquisition.

Declaration of generative AI and AI-assisted technologies in the writing process

During the preparation of this work the authors used ChatGPT in order to improve the readability and the language of the manuscript. After using this tool, the authors reviewed and edited the content as needed and take full responsibility for the content of the published article.

Declaration of competing interest

The authors declare the following financial interests/personal relationships which may be considered as potential competing interests: Mertcan Kaya reports financial support was provided by Federal Ministry for Economic Affairs and Climate Action. If there are other authors, they declare that they have no known competing financial interests or personal relationships that could have appeared to influence the work reported in this paper.

Acknowledgements

The authors would like to express their sincere gratitude to Baris Umut Kizilcelik for his valuable contribution to this project as research assistant and Manuel Hofheinz for his support in the manufacturing and post-processing of the PBF-LB/M and VPP-UVL/P test designs.

This work is supported by the BMWK 3D-Process project (project no. 03EN2065E). 3D-Process is financed by Federal Ministry for Economic Affairs and Climate Protection from Germany.

Appendix A. Supplementary material

Supplementary material related to this article can be found online at https://doi.org/10.1016/j.rineng.2025.106931.

Data availability

The data that has been used is confidential.

References

[1] K. Thulukkanam, Heat Exchanger Design Handbook, 2nd edition, CRC Press, Boca Raton, FL, USA, 2013.
[2] B. Zohuri, Heat Exchanger Types and Classifications, Springer International Publishing, Cham, 2017, pp. 19–56, Ch. 2.
[3] K. Silaipillayarputhur, Performance charts for multi-pass parallel cross-flow heat exchangers, Int. J. Mech. Eng. Robot. Res. 7 (2018) 478–482, https://doi.org/10.18178/ijmerr.7.5.478-482.
[4] J. Guo, X. Huai, K. Cheng, X. Cui, H. Zhang, The effects of nonuniform inlet fluid conditions on crossflow heat exchanger, Int. J. Heat Mass Transf. 120 (2018) 807–817, https://doi.org/10.1016/j.ijheatmasstransfer.2017.12.084.
[5] K. Zhang, W. Wei, Y. Sun, Q. Wu, M. Tang, M. Lu, Design and optimization of the inlet header structure in microchannel heat exchanger based on flow distribution uniformity, Appl. Sci. 12 (2022) 6604, https://doi.org/10.3390/app12136604.
[6] S.B. Saad, C. Gentric, J.-F. Fourmigué, P. Clément, J.-P. Leclerc, CFD and experimental investigation of the gas–liquid flow in the distributor of a compact heat exchanger, Chem. Eng. Res. Des. 92 (11) (2014) 2361–2370, https://doi.org/10.1016/j.cherd.2014.02.002.
[7] W. Zheng, W. Cai, Y. Jiang, Distribution performance of gas–liquid mixture in the shell side of spiral-wound heat exchangers, Chin. J. Chem. Eng. 27 (10) (2019) 2284–2292, https://doi.org/10.1016/j.cjche.2019.05.009.
[8] Z. Gao, X. Shang, J. Bai, Y. Yang, P. Li, Study on the uneven flow distribution and non-uniform heat transfer in microchannels, Appl. Therm. Eng. 230 (2023) 120824, https://doi.org/10.1016/j.applthermaleng.2023.120824.
[9] G. Bozzano, F. Manenti, Efficient methanol synthesis: perspectives, technologies and optimization strategies, Prog. Energy Combust. Sci. 56 (2016) 71–105, https://doi.org/10.1016/j.pecs.2016.06.001.
[10] J. Wang, Theory and practice of flow field designs for fuel cell scaling-up: a critical review, Appl. Energy 157 (2015) 640–663, https://doi.org/10.1016/j.apenergy.2015.01.032.
[11] D.A.P.S. Kumar, N. Jagadeesh, D.S. Janaki, CFD based study and optimization of manifold systems, International Research Journal of Engineering and Technology (IRJET) 5 (9) (2018) 1076–1078.
[12] F. Lu, Y. Luo, S. Yang, Analytical and experimental investigation of flow distribution in manifolds for heat exchangers, J. Hydrodyn., Ser. B 20 (2) (2008) 179–185, https://doi.org/10.1016/S1001-6058(08)60044-X.
[13] J. Wang, Pressure drop and flow distribution in parallel-channel configurations of fuel cells: Z-type arrangement, Int. J. Hydrog. Energy 35 (11) (2010) 5498–5509, https://doi.org/10.1016/j.ijhydene.2010.02.131, 3rd Argentinean and 2nd Latin American Congress in Hydrogen and Sustainable Energy Sources.
[14] M. Bassiouny, H. Martin, Flow distribution and pressure drop in plate heat exchangers—II z-type arrangement, Chem. Eng. Sci. 39 (4) (1984) 701–704, https://doi.org/10.1016/0009-2509(84)80177-3.
[15] J. Wang, H. Wang, Discrete method for design of flow distribution in manifolds, Appl. Therm. Eng. 89 (2015) 927–945, https://doi.org/10.1016/j.applthermaleng.2015.06.069.
[16] C. Wang, K. Yang, J. Tsai, I.Y. Chen, Characteristics of flow distribution in compact parallel flow heat exchangers, part II: modified inlet header, Appl. Therm. Eng. 31 (16) (2011) 3235–3242, https://doi.org/10.1016/j.applthermaleng.2011.06.003.
[17] M. Rahimi-Esbo, A.R. Sangtabi, E. Alizadeh, Manifold design in a pem fuel cell stack to improve flow distribution uniformity, Sustainability 14 (23) (2022), https://doi.org/10.3390/su142315702.
[18] O. Siddiqui, M. Al-Zahrani, A. Al-Sarkhi, et al., Flow distribution in u- and z-type manifolds: experimental and numerical investigation, Arab. J. Sci. Eng. 45 (2020) 6005–6020, https://doi.org/10.1007/s13369-020-04691-4.
[19] B. Kim, K. Kim, S. Kim, Numerical study on novel design for compact parallel-flow heat exchanger with manifolds to improve flow characteristics, Energies 13 (23) (2020) 6330, https://doi.org/10.3390/en13236330.
[20] M. Mazur, T. Bhatelia, B. Kuan, J. Patel, P.A. Webley, M. Brandt, V. Pareek, R. Utikar, Additively manufactured, highly-uniform flow distributor for process intensification, Chem. Eng. Process., Process Intensif. 143 (2019) 107595, https://doi.org/10.1016/j.cep.2019.107595.
[21] M. Li, X. Cheng, B. Yuan, J. Wei, Numerical study on the performance of a fractal vapor-liquid flow distributor, Case Stud. Therm. Eng. 40 (2022) 102537, https://doi.org/10.1016/j.csite.2022.102537.
[22] X.R. Zhuang, X.H. Xu, L. Li, X. Xin, W.F. Xu, CFD and Experimental Analyses of Flow Distribution Uniformity in Minichannel Reactors with a Bifurcation Structure

Manifold, IOP Conference Series: Earth and Environmental Science, vol. 354, IOP Publishing, 2019, 012045.

[23] H. Liu, P. Li, J.V. Lew, D. Juarez-Robles, Experimental study of the flow distribution uniformity in flow distributors having novel flow channel bifurcation structures, Exp. Therm. Fluid Sci. 37 (2012) 142–153, https://doi.org/10.1016/j.expthermflusci.2011.10.015.

[24] H. Uylings, Optimization of diameters and bifurcation angles in lung and vascular tree structures, Bull. Math. Biol. 39 (5) (1977) 509–520, https://doi.org/10.1016/S0092-8240(77)80054-2.

[25] M. Ismail, Advanced bifurcation strategies in microchannel systems: a comprehensive review of heat transfer and flow optimisation techniques, Results Eng. 24 (2024) 103564, https://doi.org/10.1016/j.rineng.2024.103564.

[26] T. Bury, M. Hanuszkiewicz-Drapała, Shaping a non-uniform inflow of mediums to enhance the performance of a double-row fin-and-tube crossflow heat exchanger, Heat Transf. Eng. 44 (11–12) (2023) 912–925, https://doi.org/10.1080/01457632.2022.2113447.

[27] J.O. Lira, H.G. Riella, N. Padoin, C. Soares, Computational fluid dynamics (CFD), artificial neural network (ANN) and genetic algorithm (GA) as a hybrid method for the analysis and optimization of micro-photocatalytic reactors: NOx abatement as a case study, Chem. Eng. J. 431 (2022) 133771, https://doi.org/10.1016/j.cej.2021.133771.

[28] Y. Koide, A.J. Kaithakkal, M. Schniewind, B.P. Ladewig, A. Stroh, P. Friederich, Machine learning for rapid discovery of laminar flow channel wall modifications that enhance heat transfer, APL Mach. Learn. 2 (1) (2024) 016108, https://doi.org/10.1063/5.0187783.

[29] K. O'Shea, R. Nash, An introduction to convolutional neural networks, arXiv:1511.08458 [abs], 2015, https://doi.org/10.48550/arXiv.1511.08458.

[30] H. Zhuang, Z. Lin, Y. Yang, K.-A. Toh, An analytic formulation of convolutional neural network learning for pattern recognition, Inf. Sci. 686 (2025) 121317, https://doi.org/10.1016/j.ins.2024.121317.

[31] O. Owoyele, P. Pal, A. Vidal Torreira, et al., Application of an automated machine learning-genetic algorithm (AutoML-GA) coupled with computational fluid dynamics simulations for rapid engine design optimization, Int. J. Engine Res. 23 (9) (2022) 1586–1601, https://doi.org/10.1177/14680874211023466.

[32] M. Gunzburger, Adjoint equation-based methods for control problems in incompressible, viscous flows, Flow Turbul. Combust. 65 (2000) 249–272, https://doi.org/10.1023/A:1011455900396.

[33] D. Gries, F.B. Schneider, Avoiding the undefined by underspecification, in: Computer Science Today: Recent Trends and Developments, Springer, Berlin Heidelberg, Berlin, Heidelberg, 1995, pp. 366–373.

[34] Y. Morita, S. Rezaeiravesh, N. Tabatabaei, R. Vinuesa, K. Fukagata, P. Schlatter, Applying Bayesian optimization with Gaussian process regression to computational fluid dynamics problems, J. Comput. Phys. 449 (2022) 110788, https://doi.org/10.1016/j.jcp.2021.110788.

[35] D. Khatamsaz, B. Vela, P. Singh, D.D. Johnson, D. Allaire, R. Arróyave, Bayesian optimization with active learning of design constraints using an entropy-based approach, npj Comput. Mater. 9 (2023) 49, https://doi.org/10.1038/s41524-023-01006-7.

[36] J.A. Paulson, C. Tsay, Bayesian optimization as a flexible and efficient design framework for sustainable process systems, Curr. Opin. Green Sustain. Chem. 51 (2025) 100983, https://doi.org/10.1016/j.cogsc.2024.100983.

[37] A. Candelieri, Mastering the exploration-exploitation trade-off in Bayesian optimization, arXiv:2305.08624, https://doi.org/10.48550/arXiv.2305.08624, 2023.

[38] A. Afzal, K.-Y. Kim, J. won Seo, Effects of Latin hypercube sampling on surrogate modeling and optimization, Int. J. Fluid Mach. Syst. 10 (3) (2017) 240–253, https://doi.org/10.5293/IJFMS.2017.10.3.240.

[39] Y.A. Çengel, J.M. Cimbala, Fluid Mechanics: Fundamentals and Applications, 3rd edition, McGraw-Hill Education, 2014.

[40] M. Kaya, C. Klahn, Sequential parameter optimization for algorithm-based design generation using data from multiphysics simulations, Proc. CIRP 119 (2023) 1234–1239, https://doi.org/10.1016/j.procir.2023.02.191, 33rd CIRP Design Conference.

[41] A. Wiberg, Design Automation for Additive Manufacturing: A Multi-Disciplinary Optimization Approach, Ph.D. thesis, Linköping University, Machine Design, Faculty of Science & Engineering, 2021.

[42] S. An, Y. Kim, O.L. Li, M. Kim, E. Yeom, Redesign for channel width to improve temperature distribution: investigation of minimum guaranteed channel width effects, Results Eng. 24 (2024) 103239, https://doi.org/10.1016/j.rineng.2024.103239.

[43] F.R. Menter, Two-equation eddy-viscosity turbulence models for engineering applications, AIAA J. 32 (8) (1994) 1598–1605, https://doi.org/10.2514/3.12149.

[44] R. Shaheed, A. Mohammadian, H.K. Gildeh, A comparison of standard k–ϵ and realizable k–ϵ turbulence models in curved and confluent channels, Environ. Fluid Mech. 19 (2018) 543–568, https://doi.org/10.1007/s10652-018-9637-1.

[45] K. Alrbaey, D. Wimpenny, R. Tosi, W. Manning, A. Moroz, On optimization of surface roughness of selective laser melted stainless steel parts: a statistical study, J. Mater. Eng. Perform. 23 (2014) 2139–2148, https://doi.org/10.1007/s11665-014-0993-9.

[46] I. Gibson, D.W. Rosen, B. Stucker, Additive Manufacturing Technologies: 3D Printing, Rapid Prototyping, and Direct Digital Manufacturing, 2nd edition, Springer, 2015.

[47] A. Wiberg, J. Persson, J. Ölvander, Design for Additive Manufacturing Using a Master Model Approach, in: International Design Engineering Technical Conferences and Computers and Information in Engineering Conference Volume 2A: 45th Design Automation Conference, 2019, V02AT03A038, https://doi.org/10.1115/DETC2019-97915.

[48] T. Chugh, Scalarizing functions in Bayesian multiobjective optimization, in: 2020 IEEE Congress on Evolutionary Computation (CEC), IEEE Press, 2020, pp. 1–8.

[49] I. Giagkiozis, P. Fleming, Methods for multi-objective optimization: an analysis, Inf. Sci. 293 (2015) 338–350, https://doi.org/10.1016/j.ins.2014.08.071.

[50] J.R.C. Dizon, C.C.L. Gache, H.M.S. Cascolan, L.T. Cancino, R.C. Advincula, Post-processing of 3D-printed polymers, Technologies 9 (2021) 61, https://doi.org/10.3390/technologies9030061.

[51] D. Thomas, The development of design rules for selective laser melting, Ph.D. thesis, University of Wales Institute, 2009.

[52] C. Klahn, B. Leutenecker-Twelsiek, Design guidelines, in: E. Pei, A. Bernard, D. Gu, C. Klahn, M. Monzón, M. Petersen, T. Sun (Eds.), Springer Handbook of Additive Manufacturing, in: Springer Handbooks, Springer International Publishing, Cham, 2023, pp. 177–198, Ch. 12.

[53] J. Kranz, Methodik und Richtlinien für die Konstruktion von laseradditiv gefertigten Leichtbaustrukturen, Springer Vieweg, Berlin, Heidelberg, 2017.

[54] F. Dadgar, H.J. Venvik, P. Pfeifer, Application of hot-wire anemometry for experimental investigation of flow distribution in micro-packed bed reactors for synthesis gas conversion, Chem. Eng. Sci. 177 (2018) 110–121, https://doi.org/10.1016/j.ces.2017.10.039.

[55] J. Cao, M. Kraut, R. Dittmeyer, L. Zhang, H. Xu, Numerical analysis on the effect of bifurcation angle and inlet velocity on the distribution uniformity performance of consecutive bifurcating fluid flow distributors, Int. Commun. Heat Mass Transf. 93 (2018) 60–65, https://doi.org/10.1016/j.icheatmasstransfer.2017.04.017.

[56] Z. Dong, Z. Wen, F. Zhao, S. Kuhn, T. Noël, Scale-up of micro- and milli-reactors: an overview of strategies, design principles and applications, Chem. Eng. Sci. X 10 (2021) 100097, https://doi.org/10.1016/j.cesx.2021.100097.

[57] S. Rott, A. Ladewig, K. Friedberger, J. Casper, M. Full, J.H. Schleifenbaum, Surface roughness in laser powder bed fusion – interdependency of surface orientation and laser incidence, Addit. Manuf. 36 (2020) 101437, https://doi.org/10.1016/j.addma.2020.101437.